Hydroxypropyl cellulose photonic architectures by soft nanoimprinting lithography

André Espinha[1], **Camilla Dore**[1], **Cristiano Matricardi**[1], **Maria Isabel Alonso**[1], **Alejandro R. Goñi**[1,2], and **Agustín Mihi**[1,*]

[1]Institut de Ciència de Materials de Barcelona, Consejo Superior de Investigaciones Científicas, Carrer dels Til·lers S/N, Campus de la UAB, 08193 Bellaterra, Barcelona, Spain

[2]Institució Catalana de Recerca i Estudis Avançats, Passeig Lluís Companys 23, 08010 Barcelona, Spain

Abstract

As contamination and environmental degradation increase nowadays, there is a huge demand for new eco-friendly materials. Despite its use for thousands of years, cellulose and its derivatives have gained renewed interest as favourable alternatives to conventional plastics, due to their abundance and lower environmental impact. We report the fabrication of photonic and plasmonic structures by moulding hydroxypropyl cellulose into sub-micrometric periodic lattices, using soft lithography. This is an alternative way to achieve structural colour in this material which is usually obtained exploiting its chiral nematic phase. Cellulose based photonic crystals are biocompatible and can be dissolved in water or not depending on the derivative employed. Patterned cellulose membranes exhibit tuneable colours and may be used to boost the photoluminescence of a host organic dye. Furthermore, we show how metal coating these cellulose photonic architectures leads to plasmonic crystals with excellent optical properties acting as disposable surface enhanced Raman spectroscopy substrates.

Sustainability is one of the fundamental challenges of modern society and in this regard, material science has been evolving towards the preferential substitution of highly contaminating materials by others with lower environmental impact. Polymeric materials are not an exception. It is estimated that the production of plastics worldwide is around 320

*Correspondence and requests for materials should be addressed to A. M. amihi@icmab.es.

Data availability
The data that support the plots within this paper and other findings of this study are available from A. M. upon reasonable request

Author contributions
A. E. and C. D. developed the concept, fabricated and characterized the samples. C. M. provided patterned PDMS moulds. A.R.G. and M.I.A. carried out PL and Raman measurements. A. E and A. M. wrote the manuscript. All authors contributed to fruitful discussions and corrected the manuscript. A. M. supervised the research.

Competing financial interests
The authors declare no competing financial interests.

Materials
Supplementary information is available in the online version of the paper. Reprints and permission information is available online at http://www.nature.com/reprints.

million tons each year and increasing,1 and only about 10% of that amount is recycled, implying an enormous generation of waste with its dramatic effects on ecosystems at the global scale. In this context, biopolymers offer an excellent alternative to common plastics due to characteristics such as large availability, low cost and biodegradability. They entail advantages in three parts of product life cycle: material harvesting, processing and fabrication, and disposal. An added value of these materials is their possible biocompatibility, which enables their use in new applications within areas such as medical or food processing. Cellulose is probably the most interesting of these biopolymers because it is the most abundant on Earth and for centuries has had a wide technological impact in areas such as textile, packaging or knowledge storage. Cellulose is a polysaccharide that results from the repetition of glucose units (Fig. S1). It is typically extracted from vegetal sources and consists of fibres with dimensions of 2 to 4 mm in length and diameters in the range of 2 to 200 μm.2 Importantly, these fibres are organized in a hierarchical structure. By further processing them by appropriate means such as mechanical, chemical or enzymatic treatments, it is possible to obtain cellulose nanoparticles (nanofibrils or nanocrystals). This nanocellulose is being actively investigated for many electronics, energy or biological applications.3, 4 Cellulose and especially nanocellulose have enabled new avenues also in the fabrication of photonic components used for example in chiral reflectors,5, 6 photonic electrodes7 or antireflection coatings in solar cells,8 multifunctional thermal9 or humidity10 responsive optical materials, flexible substrates for plasmonic sensing11 or surface enhanced Raman scattering spectroscopy.12

The typical arrangement of cellulose microfibers scatters light diffusively, providing the well-known white colour of paper. Nanocellulose instead can form compact and transparent films2 or colourful optically active ones,5 depending on the amorphous or crystalline arrangement of the particles. In suspension, it is known that cellulose and some of its derivatives may present liquid crystalline phases with bright colours.13 In particular, the observation of a mesophase in hydroxypropyl cellulose (HPC) was first reported by Werbowyj and co-workers.14 HPC has a structure similar to cellulose but some of the hydroxyl groups of the glucose building blocks are hydroxypropylated (Fig. S1). Concentrated solutions of HPC present iridescent colours and chiral behaviour due to the molecular arrangement of the linear chains in a helicoidal structure. This mesophase in HPC may be very attractive for the development of responsive systems such as recently reported strain sensors.15 In this communication, we propose an alternative route to easily provide cellulose derivatives with an optical functionality. We fabricate cellulose based two-dimensional photonic structures with sub-micrometer features and demonstrate their potential in a variety of photonic applications.

Results and discussion

Nanoimprinting Hydroxypropyl cellulose

In the search for more versatile methods for achieving structural colour in cellulose derivatives, current soft lithography techniques16 are especially suited as they have already been demonstrated useful for the fabrication of nanostructures in biopolymers.17 In comparison with traditional optical lithography they present advantages such as a low cost,

large patterned areas, good quality and reproducibility, non-diffraction-limited and compatible with roll-to-roll processing. Furthermore, while the achievement of structural colour in HPC by self-assembly is time consuming due to the requirement of molecular ordering, which may last for days or weeks, soft lithography allows for a much faster processing. For example, it has been shown that it is possible to hot emboss liquid wood18 or to use imprinting methods compatible with roll-to-roll19, 20 to structure cellulose-based polymers in a rapid way.

Concentrated HPC dilutions (above 35 wt%) may form anisotropic phases,21 however in the current work we used diluted solutions (< 20 wt%) which, additionally, are dehydrated in a fast way so that the self-assembly is hindered. As so, un-patterned regions of the samples are homogeneous, isotropic and transparent. For nanoimprinting of the HPC membranes with sub-micrometric features, the two soft lithography protocols illustrated in Fig. 1a were used. The first approach consisted in a hot embossing technique where a composite22 hard polydimethylsiloxane (h-PDMS) stamp was slightly pressed against a heated HPC membrane. In the second case – replica moulding procedure – the HPC solution was poured directly on top of the h-PDMS stamp, then dried and finally peeled off. Both methodologies produced equivalent structures on the cellulose derivative, only differing in the higher feature depth of the hot embossing approach (Fig. S2–S3). The replica moulding is more adequate for producing thick, flexible membranes while the hot embossing is preferred when highest optical quality is intended throughout the entire area of the crystal. Different kinds of lattices such as square, hexagonal or simple grooves, with different lattice parameters (L) in the submicron region may be obtained in this way, depending only on the mould used (Fig. S4–S7).

Hydroxypropyl cellulose photonic crystals

Freestanding patterned membranes were achieved after peeling-off the samples fabricated with replica moulding (Fig. 1b). Patterns with areas of (1 × 1) cm^2, with good reproducibility through the entire sample were easily produced. Moreover, the patterned films performed as photonic crystals, presenting the characteristic iridescent colour. Another attractive feature is their flexibility (Fig. 1c) and therefore the potential transferring them to other surfaces in a conformal way. The possibility of retaining a rigid or flexible substrate underneath, accomplished with hot embossing, is also useful for enhancing mechanical stability and ease of inspection of the optical properties on a flat surface. One major advantage of these photonic crystals is their biodegradability inherited from the HPC material. In fact, they can be washed away just by immersing them in water (Fig. 1d).

Although fast solubility in water is a very attractive feature for environmental purposes, some strategies may be adopted for obtaining cellulose based insoluble photonic films. Fig. 1d–f compares the different behaviour of three different cellulose-based membranes in water. Bare HPC based films completely dissolved after being immersed in water for approximately 30 s (Fig. 1d). A step towards enhanced stability was the use of crosslinked HPC membranes (Fig. 1e). The crosslinking was achieved by adding divinyl sulfone to the HPC solution in water and increasing its pH with sodium hydroxide, before carrying out the soft lithographic step. The result is a patterned hydrogel,23 that becomes white upon water

Europe PMC Funders Author Manuscripts

immersion due to the increased light scattering coming from the nanopores swelling in the film. Incidentally, this system is a fast and visual humidity sensor by undergoing the dramatic transition from colourful to white aspect. Finally, full mechanical stability under water could be achieved by imprinting a non-soluble cellulose derivative – acetyl cellulose (Fig. S1) (AC). In this case, it is possible to obtain a non-degradable photonic film that retains its iridescence after immersion in water for 60 s (Fig. 1f).

Nanoimprinting is a versatile strategy that allows the fabrication of HPC photonic crystal films operating at spectral ranges determined by their geometry. The different colours exhibited by the films depend on the structure, topology or lattice parameter imprinted. To exemplify the structural colour functionality and characterize the optical properties of the HPC photonic crystal membranes, a set of samples with square lattice and varying *L* was tested. Photographs of the samples under normal incidence to the films (Fig. 2a) clearly showed the change from blue to green to red, as *L* was increased from 400 nm to 500 nm to 600 nm, in agreement with the colour observed at the optical microscope (Fig. 2b). The SEM analysis confirmed the good replication of the square array of holes, 300 nm in diameter and 220 nm in depth, for the three lattice parameters studied (Fig. 2c) – larger area images may be found in the Supporting Information (Fig. S4). Characterization of the reflectance by FTIR spectroscopy (Fig. 2d) revealed a peak centred at 430 nm, 550 nm or 680 nm for each sample respectively, in good agreement with simulations performed by finite-difference time domain (FDTD) calculations, also shown in the figure. It is important to highlight that the colours observed in these solid crystals arise from the 2D patterned surface, in contrast to the colour achieved by the presence of anisotropic phases in concentrated HPC dispersions in water.

Hydroxypropyl cellulose plasmonic crystals

Enhanced optical properties and further functionality can be achieved by metal coating the cellulose based photonic membranes. Such plasmonic crystals were produced by thermal evaporation of 50 nm of silver on top of HPC gratings. In doing so, the optical properties of these samples result from the combination of photonic and plasmonic modes. In plasmonic crystals, light fulfilling the condition of Bragg diffraction imposed by the lattice launches surface plasmon polaritons (SPPs), where strong electric fields at the surface of the metal can be used to enhance any light mater interaction. Plasmonic crystals have been used in the literature to enhance light emission,24 amplify light absorption in photodetectors,25 or to produce structural colour in metallic surfaces.26, 27

Due to the negative dielectric permittivity of the metal, the overall refractive index contrast of the system is enhanced giving origin to much more vivid colours in the cellulose based plasmonic crystals than in their dielectric counterparts (Fig. 3a). Moreover, the samples keep the original flexibility (Fig. 3b). Optical characterization of plasmonic crystals consisting in a hexagonal lattice of imprinted nanoholes (Fig. 3c), revealed extinction peaks with up to 80% derived from the presence of the nanopatterns. These peaks correspond to the excitation of Bragg surface plasmon polaritons (Bragg-SPP) and as *L* is increased, the resonances redshift accordingly. Both the position and the intensity of the Bragg-SPP agreed

significantly well with theoretical simulations performed by FDTD calculations (dashed curves of the figure).

As pointed out before, a major advantage of the fabrication methods used in this work is the possibility of imprinting HPC on top of different substrates. For providing additional functionality to the photonic and plasmonic crystals we tested the fabrication of our plasmonic architectures using regular paper as substrate. HPC was coated on top of a piece of paper and then nanoimprinted, followed by metal evaporation. As illustrated by the SEM images (Fig. 3d and Fig. 3e), the patterns were transferred with extreme good quality also in this case. This particular example demonstrates the potential of the proposed system for functioning as a colourful photonic ink28 in applications such as anti-counterfeiting technology, packaging or decorative paper. In fact, intense colours were easily achieved without the use of any expensive or toxic chemical pigment and in all cases, the photonic crystal presented a good adhesion to the paper substrate as the HPC infiltrated the porous cellulose fibres of the paper sheet (Fig. S8). This method could be adapted to other kinds of paper or cardboard with notable industrial impact.

HPC plasmonic crystals for photoluminescence enhancement

Plasmonic architectures have been sought as a way to modify and enhance the emission of light sources.26 The performance of HPC based plasmonic crystals was further tested by doping HPC with an organic dye – Rhodamine B (RhB). This dye is attractive due to its high quantum yield and has already been used for doping biopolymers such as silk29 or polydiolcitrates.30 The samples as viewed from the HPC side exhibited the characteristic magenta colour of RhB whereas inside the patterned areas strong iridescence was observed, as in bare plasmonic crystals (Fig. 3f). Measurements of photoluminescence (PL) were done on these crystals (see section 5 of SI), according to scheme on Fig. 3g, comparing the emission from nanopatterned regions and flat regions. An example is presented for a hexagonal plasmonic crystal of L = 800 nm (Fig. 3h). The detected PL for regions inside the patterned area was approximately ten-fold the signal detected in the reference flat area. RhB has a high quantum yield (close to 70%) and in the proposed system, the plasmonic structure provided a more efficient way to extract light from the membrane.

HPC plasmonic crystals for SERS sensing

Once characterized the optical properties of the HPC plasmonic crystal membranes, we investigate now the use of these architectures as disposable substrates for the detection of surface enhanced Raman scattering (SERS). Raman sensing is one of the fields where plasmonics has had the greatest impact. The use of plasmonic resonances greatly amplifies the Raman scattering from the analyte, leading to its identification, even in scarce amounts. Patterned HPC membranes with hexagonal lattice and pillar morphology (L = 700 nm) were fabricated using the replica moulding technique previously explained. Afterwards, they were silver coated by thermal evaporation (100 nm). A representative extinction spectrum of the samples is shown in Fig. 4a. The optical characterization of these architectures revealed an extinction peak attributed to the excitation of a plasmonic resonance sustained by the architecture. In order to assess the SERS performance of these substrates, the samples were functionalized with thiophenol via vapor phase and analysed (Fig. S10). Thiophenol (inset

Fig. 4b) is a well-known Raman probe that easily binds to metal surfaces. Its characteristic vibrational modes are positioned at 1001 cm^{-1}, 1026 cm^{-1}, 1094 cm^{-1} and 1586 cm^{-1}.31 These modes could be clearly identified in the spectra taken from the probe adsorbed to the surface of our plasmonic crystals (Fig. 4b). Interestingly, the geometry employed in our plasmonic crystals was suitable for the excitation of plasmonic resonances which in turn, facilitated the use of these membranes as SERS substrates, active at different excitation wavelengths (λ = 532 and 633 nm). When comparing spectra collected from the flat regions of the substrate (grey curves in the figure) with the spectra collected inside the patterns, a clear enhancement of the signal was observed.

SERS is a phenomenon characterized by the presence of hotspots at the dielectric/metal interface. These are spatial regions with extremely intense electric field.31 The Raman signal measured is originated by the effect of these hot spots on the molecules placed therein. There is great interest in the imaging of the above mentioned hot spots, to identify the active sensing regions of the SERS substrate. Here we demonstrate how the excellent quality of our HPC plasmonic crystal membranes enables the identification of the hot spots for the two laser frequencies employed. First off, electron microscopy images (Fig. 4c) and optical microscopy images (Fig. 4d) were used to illustrate the hexagonal array of Ag coated pillars forming the plasmonic substrate. Second, Raman spectroscopy maps were performed by scanning the signal throughout the surface and monitoring the Raman peak of thiophenol at 1578 cm^{-1} (Fig. 4e), for both laser frequencies. The Raman signal map for the 532 nm laser excitation revealed that the majority of the signal came from the regions located between the metallic pillars. On the contrary, when the sample was illuminated with the 633 nm laser, coinciding with the extinction peak, the Raman signal was originated at the pillars themselves. This observation was further corroborated with numerical simulations, were the position of the extinction peak was fitted and the spatial distribution of the electric field intensity at both laser frequencies reproduced (Fig. 4f and Fig. S12). Whereas at λ = 532 nm the electric field distribution revealed the presence of an extended mode, λ = 633 nm corresponded to a hybrid mode where the electric field was concentrated mostly at the top of the pillars. The good agreement between simulations and Raman measurement maps demonstrated that we were capable of imaging the spatial distribution of hot spots in our plasmonic structures for two different resonant optical modes. Moreover, they demonstrate the importance of the imprinted nanostructure for enhancing the Raman signal.

Conclusions

In summary, we have shown how to produce photonic and plasmonic crystal thin films out of hydroxypropyl cellulose. The resulting structures incorporate the biocompatibility and biodegradability aspects inherited form the cellulose derivative used. Following recent tendencies that are exploring materials for transient electronics,32, 33 our system opens a wide range of potential applications in transient photonics. Two routes were presented to integrate these photonic architectures in applications: to produce freestanding flexible samples that may be transferred to other surfaces; or to directly nanoimprint a HPC coating on the desired substrate. HPC nanoimprinted crystals are a very convenient platform for the realization of plasmonic systems by simply metal coating the HPC photonic membranes. Different morphologies and topologies were produced with this method, both free standing

or on top of functional substrates. These samples offer a convenient opportunity for the production of colour in packaging systems or in photonic papers30 and they could accomplish the function of washable and edible34 detectors or labels in food industry. In fact, HPC is an excellent candidate for such matters due to its already established applicability as drug excipient or ophthalmic lubricant.35 Moreover, we explored the possibility of doping HPC with an organic dye to achieve a luminescent system. It was made evident that the plasmonic crystal improved the out-coupling of light, enhancing the photoluminescence signal by a tenfold factor with respect to a flat reference. Finally, HPC based plasmonic crystals in the context of surface enhanced Raman spectroscopy (SERS) were tested. An enhancement of Raman signal due to the presence of the nanostructure determined by the underneath HPC surface was demonstrated.

Methods

Chemicals

Hard polydimethylsiloxane kit was acquired from Gelest and soft poly-dimethylsiloxane Sylgard 184 kit from Dow Corning Corporation. 1H,1H,2H,2H-Perfluoro-octyltrichlorosilane, 97% was purchased from Alfa Aesar. Acetone, Divinyl sulfone, Acetyl cellulose with average M_w = 30 kDa and Hydroxypropyl cellulose with average M_w = 100 kDa were acquired from Sigma-Aldrich. All chemicals were used as received.

Stamps preparation

Composite bilayer stamps constituted by a thin h-PDMS layer for ensuring good pattern replica and mechanical stability, and a thick soft PDMS (s-PDMS) layer to allow their manipulation were prepared according to previously reported methods.22

Nanoimprinting of cellulose derivatives

A HPC solution in water was prepared by adding 23 ml of deionized water to 5 g of HPC powder. The solution was intensively stirred and reserved for use in a sealed vial. Regarding the replica moulding procedure, the HPC solution was poured on top of a h-PDMS mould and spin coated at 500 rpm with an initial acceleration of 100 rpm min s^{-1}. Once finished, the membranes were peeled-off to obtain freestanding samples. For hot embossed samples, a dilution of the original HPC at a new concentration of 41 mg ml^{-1} was initially prepared. Then thin films were prepared by spin coating (parameters: acceleration ramp of 1000 rpm s^{-1}, duration of 60 s at 3500 rpm), on top of glass slides or silicon wafers as substrate. The samples were heated at 140°C and imprinted with the h-PDMS mould by applying a light pressure during approximately 30 s. Finally, the h-PDMS was demoulded. In case of samples produced with the crosslinker, a solution of NaOH in water was first prepared at a concentration of 1 mg ml^{-1}. A HPC mass of 0.16 g was added to a volume of 1.808 ml of the NaOH solution and magnetically stirred overnight. A divinyl sulfone mass of 0.032 g were added to the mixture and stirred for a few more minutes. The replica moulding process repeated. Insoluble photonic membranes were prepared by mixing 0.16 g of acetylcellulose in 1.832 ml of acetone, magnetically stirring overnight and repeating the replica moulding procedure. Silver films were deposited on top of HPC membranes using a MBRAUN

thermal evaporator. The chamber pressure was 4×10^{-7} bar and an evaporation rate of 10 nm min^{-1} was used.

Photoluminescence measurements

The PL was excited using either the 405 nm line of a continuous wave laser diode or the 514 nm line of an Ar^{+}-ion gas laser. The PL signal was collected using an Olympus microscope with a 20 × objective (NA = 0.35) in backscattering geometry. The microscope was coupled to a high throughput and high resolution LabRam HR800 spectrometer using a grating of 600 lines/mm and equipped with a liquid nitrogen cooled charge coupled device (CCD) detector. A scheme of the experimental setup is provided in Fig. S9. All measurements were performed at room temperature.

Raman spectroscopy measurements

The initially freestanding membranes were transferred to a flat PDMS block so that their surface was free from wrinkles or curving. Raman images were obtained at ambient conditions and in backscattering geometry using the WITec Alpha300 R confocal setup. For excitation either a frequency-doubled Nd:YAG laser emitting at 532 nm or a He-Ne gas laser (633 nm) was coupled into a Zeiss microscope through a wavelength-specific single-mode fibre and collimated by an achromatic lens. The beam was focused onto the sample, with power 0.25 mW, using a Zeiss EC Epiplan-Neofluar (100 ×, 0.9 NA) objective, giving an estimated spot size of 0.35 μm (green) or 0.43 μm (red). The pixel size for the images was (0.1×0.1) μm^2, given by the scanning movement of a piezo-motor-driven sample stage. The collected light was focused into a multimode optical fibre, which served as the entrance slit for the spectrometer. The 3.5 μm diameter single-mode input fibre and the 50 μm diameter multimode output fibre provided the optical apertures for the confocal arrangement. A Si back-illuminated 1024 × 127 pixel CCD cooled at −60 °C was used for detection. Using gratings of 600 grooves/mm with blaze at 500 nm (green) and of 300 grooves/mm with blaze at 750 nm (red), complete Raman spectra in the interesting spectral range (from about 200 to 3500 cm^{-1}) were acquired at each image pixel using integration times of 0.1 s with sub-micron spatial resolution (Fig. S10). Images were analysed using WITec Project FOUR software.

Theoretical modelling

A commercial-grade simulator based on the finite-difference time-domain method was used to perform the calculations (Lumerical Solutions, Inc., https://www.lumerical.com/tcad-products/fdtd). For simulating the thick freestanding HPC membranes, 120 reflectance spectra for different thicknesses were calculated and averaged so that oscillations due to Fabry-Perot interference were averaged. A mesh refinement of 5 nm was used in all structures. Transmittance (T) and reflectance (R) were calculated and extinction as $1 - R - T$. The simulations were performed for both polarizations and averaged to reproduce unpolarized light (Fig. S12).

Supplementary Material

Refer to Web version on PubMed Central for supplementary material.

Acknowledgements

The authors would like to acknowledge M. Simón and A. Gómez for AFM measurements. The Spanish Ministerio de Economía, Industria y Competitividad (MINECO) is gratefully acknowledged for its support through Grant No. SEV-2015-0496 in the framework of the Spanish Severo Ochoa Centre of Excellence program and also for its support through Grant MAT2016-79053-P. AM was funded by a Ramón y Cajal fellowship (RYC-2014-16444). This project has received funding from the European Research Council (ERC) under the European Union's Horizon 2020 research and innovation programme (grant agreement No 637116, ENLIGHTMENT).

References

1. Plastics – the Facts 2016. http://www.plasticseurope.org
2. Hoeng F, Denneulin A, Bras J. Use of nanocellulose in printed electronics: a review. Nanoscale. 2016; 8:13131–13154. [PubMed: 27346635]
3. Lagerwall J, et al. Cellulose nanocrystal-based materials: from liquid crystal self-assembly and glass formation to multifunctional thin films. NPG Asia Mater. 2014; 6:e80.
4. Zhu H, et al. Wood-Derived Materials for Green Electronics, Biological Devices, and Energy Applications. Chem Rev. 2016; 116:9305–9374. [PubMed: 27459699]
5. Dumanli A, et al. Controlled, Bio-inspired Self-Assembly of Cellulose-Based Chiral Reflectors. Adv Optical Mater. 2014; 2:646–650.
6. Fernandes S, et al. Mind the Microgap in Iridescent Cellulose Nanocrystal Films. Adv Mater. 2017; 29:1603560.
7. Águas H, et al. Thin Film Silicon Photovoltaic Cells on Paper for Flexible Indoor Applications. Adv Funct Mater. 2015; 25:3592–3598.
8. Ha D, Fang Z, Hu L, Munday J. Paper-Based Anti-Reflection Coatings for Photovoltaics. Adv Energy Mat. 2014; 4:1301804.
9. Espinha A, et al. Shape Memory Cellulose-Based Photonic Reflectors. ACS Appl Mater Inter. 2016; 8:31935–31940.
10. Wu T, et al. A bio-inspired cellulose nanocrystal-based nanocomposite photonic film with hyper-reflection and humidity-responsive actuator properties. J Mater Chem C. 2016; 4:9687–9696.
11. Polavarapu L, Liz-Marzán L. Towards low-cost flexible substrates for nanoplasmonic sensing. Phys Chem Chem Phys. 2013; 15:5288–5300. [PubMed: 23303134]
12. Tian L, et al. Bacterial Nanocellulose-Based Flexible Surface Enhanced Raman Scattering Substrate. Adv Mater Interfaces. 2016; 3:1600214.
13. Gilbert R, Patton P. Liquid crystal formation in cellulose and cellulose derivatives. Prog Polym Sci. 1983; 9:115–131.
14. Werbowyj R, Gray D. Liquid Crystalline Structure In Aqueous Hydroxypropyl Cellulose Solutions. Mol Cryst Liq Cryst. 1976; 34:97–103.
15. Kamita G, et al. Biocompatible and Sustainable Optical Strain Sensors for Large-Area Applications. Adv Optical Mater. 2016; 4:1950–1954.
16. Xia Y, Whitesides G. Soft lithography. Angew Chem Int Ed. 1998; 37:550–575.
17. Espinha A, Serrano M, Blanco A, López C. Thermoresponsive Shape-Memory Photonic Nanostructures. Adv Optical Mater. 2014; 2:516–521.
18. Worgull M, et al. Hot embossing and thermoforming of biodegradable three-dimensional wood structures. RSC Adv. 2013; 3:20060–20064.
19. Mäkelä T, Kainlauri M, Willberg-Keyriläinen P, Tammelin T, Forsström U. Fabrication of micropillars on nanocellulose films using a roll-to-roll nanoimprinting method. Micro Engn. 2016; 163:1–6.
20. Mäkelä T, Haatainen T, Ahopelto J. Roll-to-roll printed gratings in cellulose acetate web using novel nanoimprinting device. Micro Engn. 2011; 88:2045–2047.
21. Werbowyj R, Gray D. Optical properties of hydroxypropyl cellulose liquid crystals. I. Cholesteric pitch and polymer concentration. Macromolecules. 1984; 17:1512–1520.
22. Odom T, Love J, Wolfe D, Paul K, Whitesides G. Improved Pattern Transfer in Soft Lithography Using Composite Stamps. Langmuir. 2002; 18:5314–5320.

23. Kabra B, Gehrke S, Spontak R. Microporous, Responsive Hydroxypropyl Cellulose Gels. 1. Synthesis and Microstructure. Macromolecules. 1998; 31:2166–2173.
24. Yang A, et al. Unidirectional Lasing from Template-Stripped Two-Dimensional Plasmonic Crystals. ACS Nano. 2015; 9:11582–11588. [PubMed: 26456299]
25. de Arquer F, Mihi A, Konstantatos G. Large-Area Plasmonic-Crystal-Hot-Electron-Based Photodetectors. ACS Photonics. 2015; 2:950–957.
26. James T, Mulvaney P, Roberts A. The Plasmonic Pixel: Large Area, Wide Gamut Color Reproduction Using Aluminum Nanostructures. Nano Lett. 2016; 16:3817–3823. [PubMed: 27164410]
27. Cheng F, Gao J, Luk T, Yang X. Structural color printing based on plasmonic metasurfaces of perfect light absorption. Sci Rep. 2015; 5:11045. [PubMed: 26047486]
28. Fudouzi H, Xia Y. Photonic Papers and Inks: Color Writing with Colorless Materials. Adv Mater. 2003; 15:892–896.
29. Min K, Kim S, Kim C, Kim S. Colored and fluorescent nanofibrous silk as a physically transient chemosensor and vitamin deliverer. Sci Rep. 2017; 7:5448. [PubMed: 28710484]
30. Espinha A, Serrano M, Blanco A, López C. Random Lasing in Novel Dye-Doped White Paints with Shape Memory. Adv Optical Mater. 2015; 3:1080–1087.
31. Macias G, Alba M, Marsal L, Mihi A. Surface roughness boosts the SERS performance of imprinted plasmonic architectures. J Mater Chem C. 2016; 4:3970–3975.
32. Hwang S, et al. A Physically Transient Form of Silicon Electronics. Science. 2012; 337:1640–1644. [PubMed: 23019646]
33. Bae H, et al. Physically Transient Memory on a Rapidly Dissoluble Paper for Security Application. Sci Rep. 2016; 6:38324. [PubMed: 27917910]
34. Tao H, et al. Silk-Based Conformal, Adhesive, Edible Food Sensors. Adv Mater. 2012; 24:1067–1072. [PubMed: 22266768]
35. Luchs J, Nelinson D, Macy J. Efficacy of Hydroxypropyl Cellulose Ophthalmic Inserts (LACRISERT) in Subsets of Patients With Dry Eye Syndrome: Findings From a Patient Registry. Cornea. 2010; 29:1417–1427. [PubMed: 20847657]

Europe PMC Funders Author Manuscripts

Europe PMC Funders Author Manuscripts

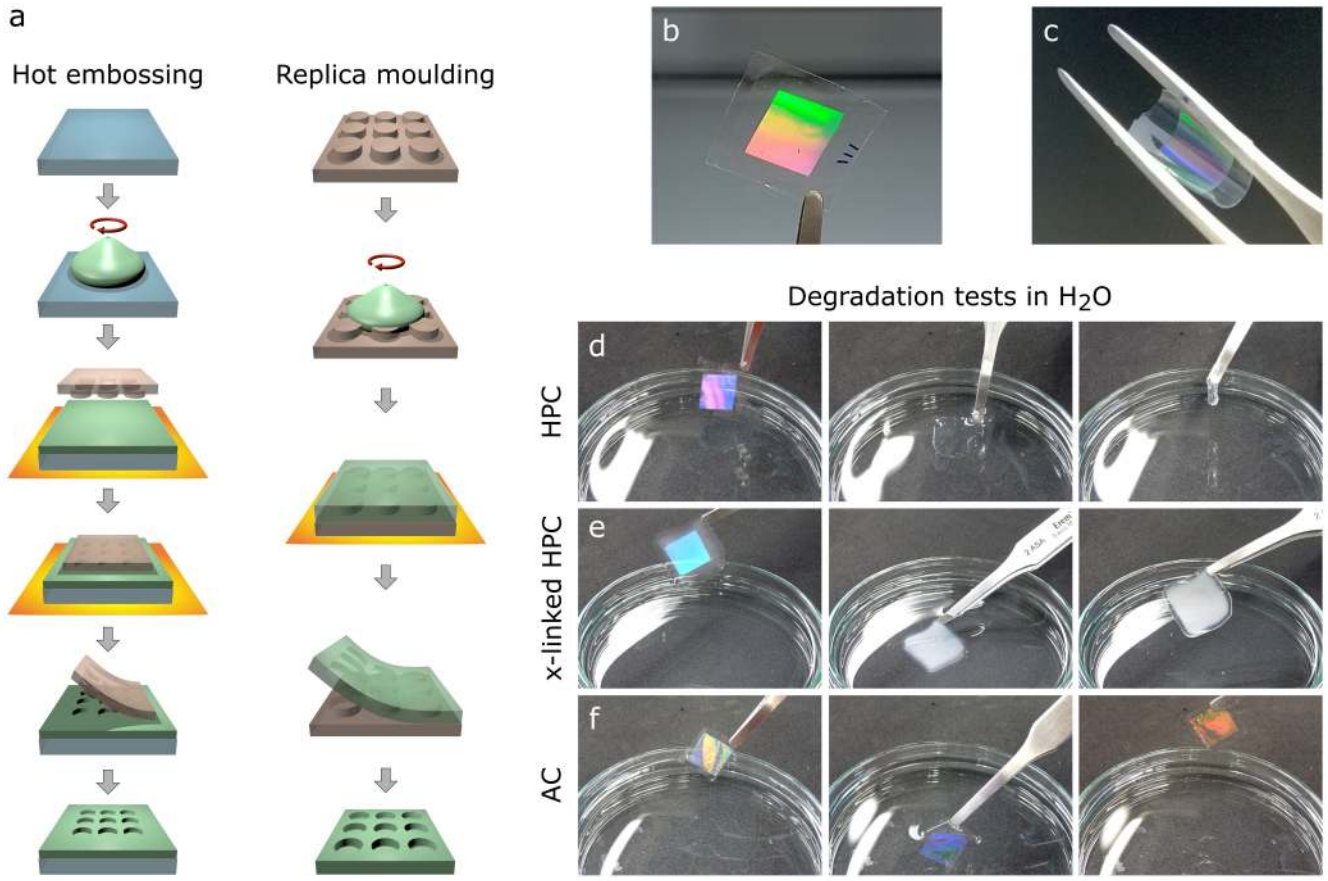

Figure 1. Fabrication procedures and water solubility tests of cellulose photonic crystal films.

a, Scheme illustrating the hot embossing and replica moulding procedures used for the fabrication of cellulose based photonic thin films and membranes. **b**, Exemplar image of a freestanding hydroxypropyl cellulose (HPC) photonic crystal – lateral size of the imprinted area is 1 cm. **c**, Exemplar image of the flexibility exhibited by a self-standing HPC photonic film. **d**, Sequence of photos illustrating the facile solubility of HPC photonic membranes in water. **e**, Sequence of photos showing the pattern loss of crosslinked HPC (×-linked HPC) in water. **f**, Sequence of photos exemplifying the stability of patterned acetyl cellulose (AC) films in water.

Europe PMC Funders Author Manuscripts

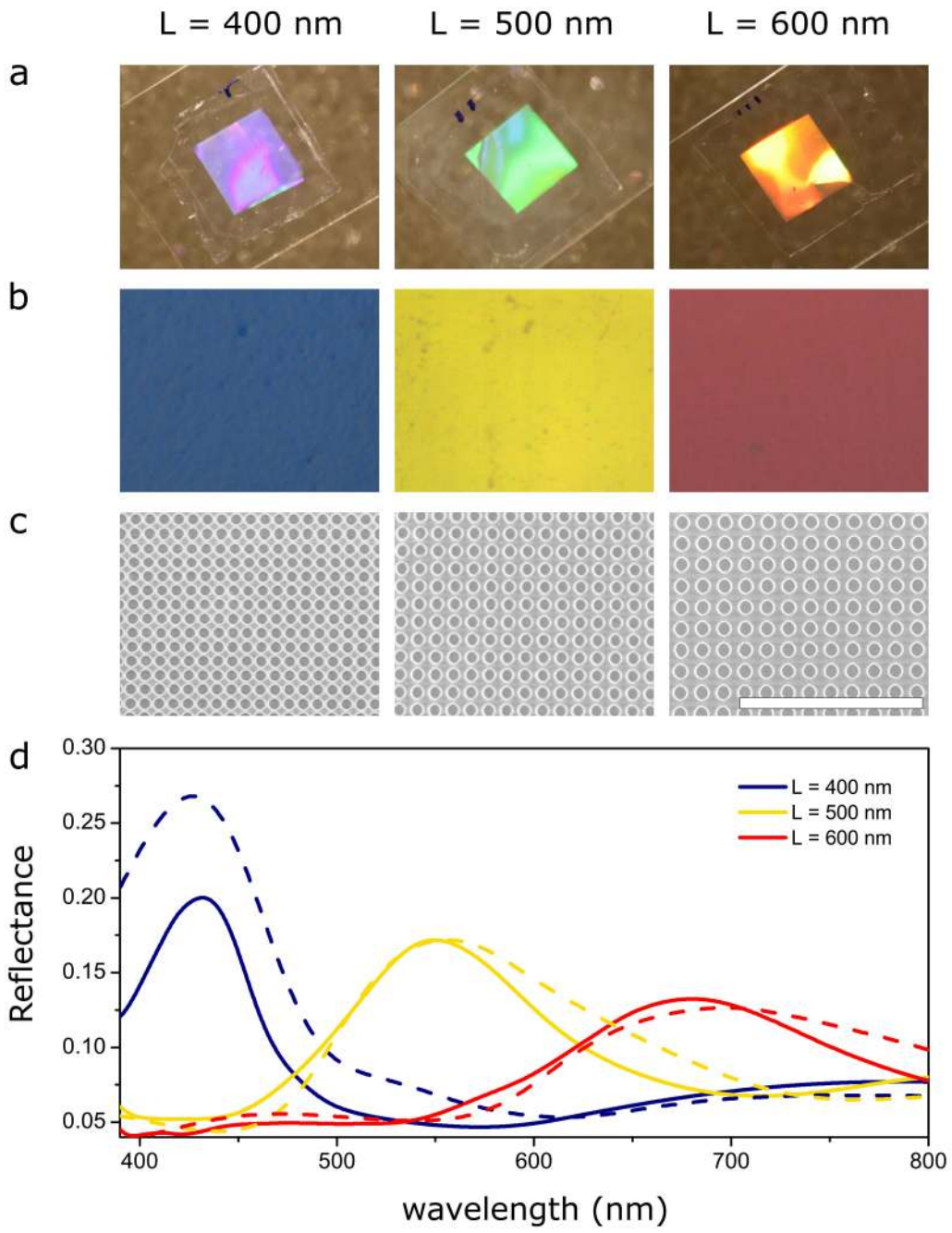

Figure 2. Cellulose based photonic crystals.

a, Photographs of the HPC photonic films (square lattice of imprinted cylindrical holes), for lattice parameters of 400, 500 and 600 nm – square lateral size is 1 cm. **b**, Images of the HPC photonic films acquired with an optical microscope (4X objective, NA 0.1). **c**, SEM micrographs of the HPC photonic films (top view) – scale bar corresponds to 5 μm. **d**, Specular Reflectance characterization of the samples – solid curves, along with theoretical modelling of the structures by FDTD calculations – dashed curves.

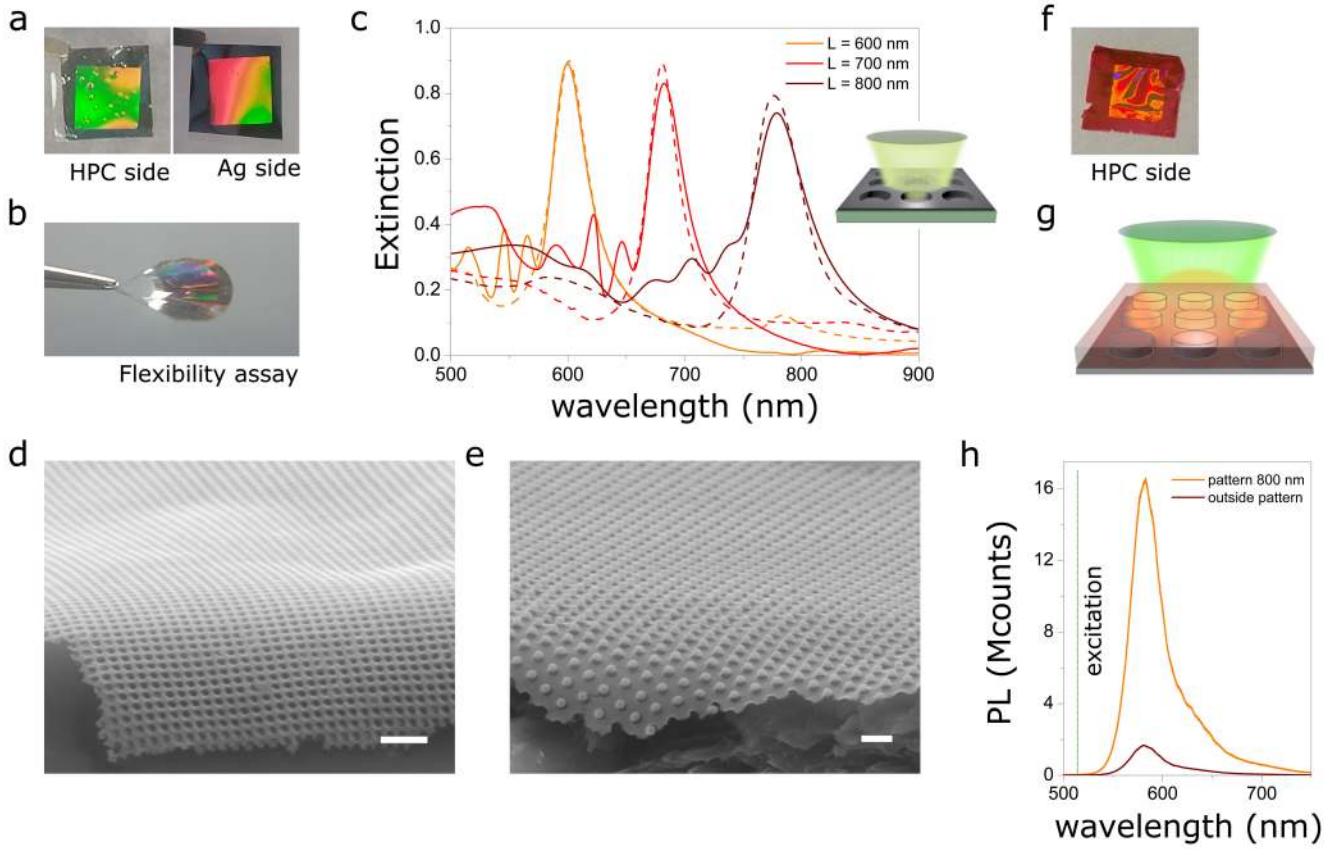

Figure 3. Cellulose based plasmonic crystals.

a, Picture of both sides of a plasmonic crystal made of silver (50 nm) deposited on a HPC patterned membrane **b**, Example of plasmonic crystals flexibility. **c**, Experimental (solid lines) and simulated (dash lines) optical extinction spectra of HPC-based plasmonic crystals (hexagonal array of holes, L = 600, 700 and 800 nm). Inset displays the measurement scheme (sample studied from the metal side). **d**, SEM lateral view of a HPC plasmonic crystal on a paper substrate – square lattice of imprinted holes; scale bar corresponds to 1 μm. **e**, Similar view of a hexagonal lattice of imprinted pillars; scale bar corresponds to 1 μm. **f**, Image of a plasmonic crystal fabricated with RhB-doped HPC. **g**, Scheme of photoluminescence measurements showing light impinging the HPC face. **h**, Comparison between PL spectrum of RhB in a patterned area - hexagonal plasmonic crystal (L = 800 nm) and a planar reference.

Europe PMC Funders Author Manuscripts

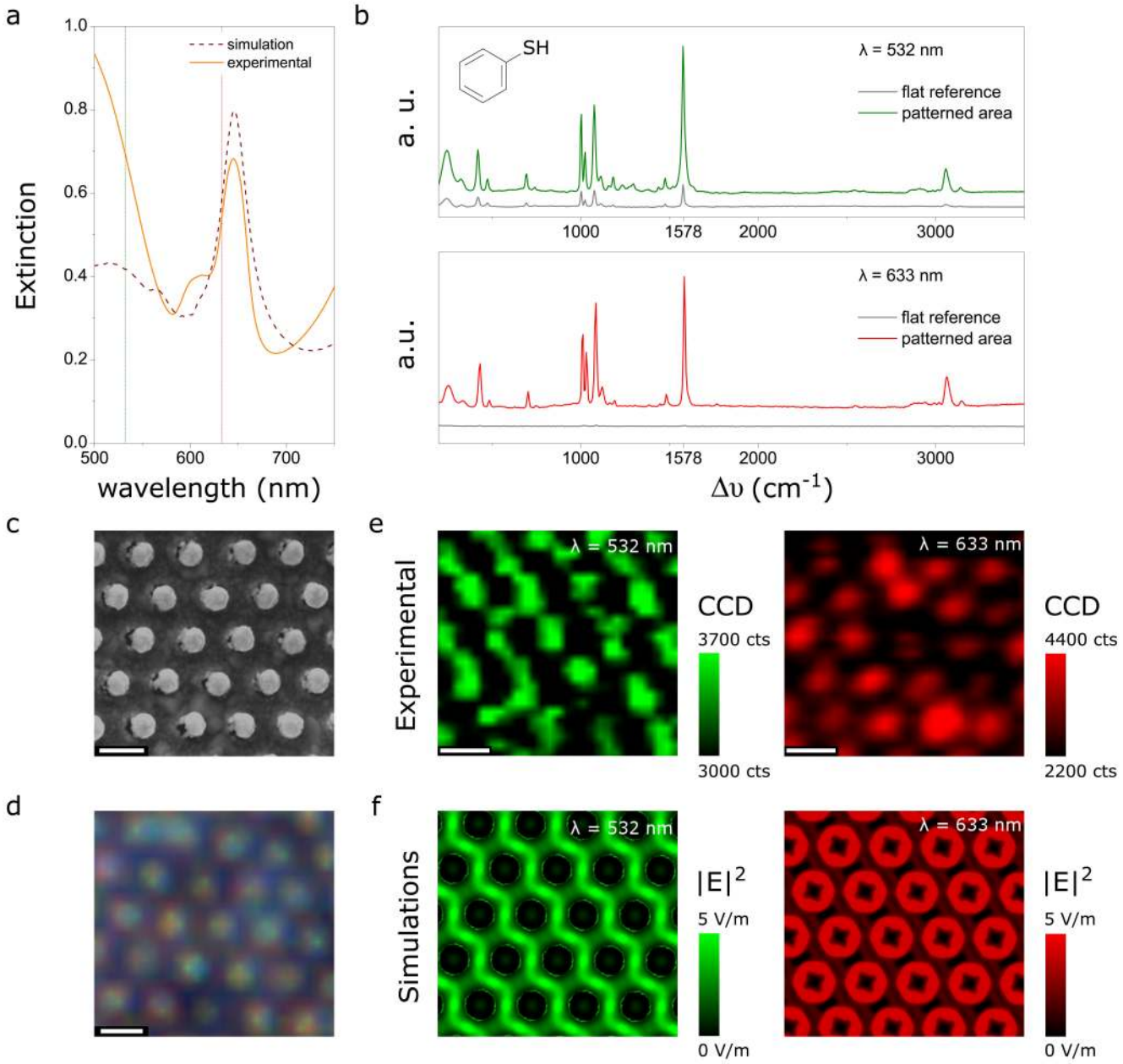

Figure 4. HPC Plasmonic crystal membranes as SERS substrates.

a, Representative extinction spectrum of a silver coated HPC hexagonal lattice of pillars (*L* = 700 nm) – experimental results (solid curve) and FDTD simulation (dashed curve). **b**, Raman spectra of thiophenol (inset) collected in reference flat areas (grey curves) and in HPC/Ag patterned substrates, for excitation wavelengths of 532 and 633 nm; curves were vertically displaced for convenience. **c**, Representative SEM image of the sample – scale bar corresponds to 600 nm. **d**, Representative optical microscopy image of the sample observed with a 100 × magnification objective used to measure Raman maps – scale bar corresponds to 600 nm. **e**, Raman maps of the surface, monitoring the intensity of the peak at 1578 cm^{-1}, for excitation wavelengths of 532 nm (left) and 633 nm (right); scale bar corresponds to 600

Europe PMC Funders Author Manuscripts

nm. **f**, FDTD theoretical simulations of the electric field spatial distributions for the corresponding wavelengths.

Europe PMC Funders Author Manuscripts